

# Journal of Materials Chemistry A

Accepted Manuscript



This is an *Accepted Manuscript*, which has been through the Royal Society of Chemistry peer review process and has been accepted for publication.

*Accepted Manuscripts* are published online shortly after acceptance, before technical editing, formatting and proof reading. Using this free service, authors can make their results available to the community, in citable form, before we publish the edited article. We will replace this *Accepted Manuscript* with the edited and formatted *Advance Article* as soon as it is available.

You can find more information about *Accepted Manuscripts* in the [Information for Authors](#).

Please note that technical editing may introduce minor changes to the text and/or graphics, which may alter content. The journal's standard [Terms & Conditions](#) and the [Ethical guidelines](#) still apply. In no event shall the Royal Society of Chemistry be held responsible for any errors or omissions in this *Accepted Manuscript* or any consequences arising from the use of any information it contains.

Cite this: DOI: 10.1039/c0xx00000x

www.rsc.org/xxxxxx

ARTICLE TYPE

**MgFePO<sub>4</sub>F as a feasible cathode material for magnesium batteries**Zhen-Dong Huang<sup>a,\*</sup>, Titus Masese<sup>a</sup>, Yuki Orikasa<sup>a</sup>, Takuya Mori<sup>a</sup>, Taketoshi Minato<sup>b</sup>, Cedric Tassel<sup>c</sup>, Yoji Kobayashi<sup>c</sup>, Hiroshi Kageyama<sup>c</sup>, Yoshiharu Uchimoto<sup>a</sup>

Received (in XXX, XXX) Xth XXXXXXXXX 20XX, Accepted Xth XXXXXXXXX 20XX

DOI: 10.1039/b000000x

A stoichiometric MgFePO<sub>4</sub>F (MFPF) is synthesised by using a solid-state carbothermal method. Its monoclinic framework, possessing an entire cationic mixing of Mg<sup>2+</sup> and Fe<sup>2+</sup>, is validated via both crystal structure analysis and simulation. Interestingly, MFPF exhibits a relatively high potential (~2.6 V vs. Mg/Mg<sup>2+</sup>) and good cyclic stability with an encouraging capacity (~53mAhg<sup>-1</sup>), bringing to the fore MFPF as a promising cathode material for magnesium batteries.

Lately, the high price (~69000 \$·ton<sup>-1</sup>)<sup>1</sup> and low abundance (~7 × 10<sup>-4</sup> %)<sup>2</sup> of lithium is viewed as an impediment to the further large-scale application of lithium ion batteries (LIBs). To meet the ever-increasing demand on large-scale energy storage/conversion devices, paramount attention has been paid to develop alternative rechargeable battery systems based on magnesium, as they are of much lower cost (3020 \$·ton<sup>-1</sup>), much higher abundance (13.9%)<sup>2</sup> and exhibit higher theoretical volumetric energy density (3832 mAh·cm<sup>-3</sup>) than Li (2062 mAh·cm<sup>-3</sup>)<sup>1</sup>. Moreover, Mg is stable upon air exposure and is free of dendritic deposition during repeated cycling, thus, inherently safer than Li.<sup>1, 2</sup> A prototype Mg battery (MB) was first demonstrated in 2000,<sup>3</sup> but its feasibility strongly relies on the development of suitable cathode materials and electrolyte. Recently, more efforts have been inclined to develop a suitable Mg<sup>2+</sup> electrolyte with broad electrochemical window, while works relating to new cathode materials remain scarce.

Owing to strong Mg interactions with the anions and the cations of the hosts or to the polarization effect of Mg<sup>2+</sup> cations with a high charge/radius ratio, the intrinsically slow solid-state diffusion kinetics of Mg<sup>2+</sup> hampers most of the intercalation compounds as cathodes for MBs.<sup>1</sup> Up to date, only few cathode materials, such as the Chevrel phases Mg<sub>x</sub>Mo<sub>6</sub>T<sub>8</sub> (T=S, Se),<sup>4, 5</sup> Mg<sub>x</sub>MSiO<sub>4</sub> (M = Fe,<sup>6</sup> Mn,<sup>7, 8</sup> Co<sup>9</sup>), transition metal oxides (such as V<sub>2</sub>O<sub>5</sub><sup>10, 11</sup> and MnO<sub>2</sub><sup>12, 13</sup>) and metal chalcogenides (such as MoS<sub>2</sub>,<sup>14, 15</sup> TiS<sub>2</sub><sup>16</sup> and WSe<sub>2</sub><sup>17</sup>), have been proven to be plausible (de) intercalation hosts of Mg<sup>2+</sup>. A majority of research works have been directed toward the synthesis of nanostructured cathode materials in order to reduce the diffusion distance of Mg<sup>2+</sup>. However, only few works have been directed toward evaluating the feasibility of using new compounds as possible cathodes for MBs. This is the focus in this study.

Fluoro-polyanionic cathode materials, such as Na<sub>2</sub>FePO<sub>4</sub>F,<sup>18</sup> LiFePO<sub>4</sub>F,<sup>19</sup> and LiVPO<sub>4</sub>F,<sup>20</sup> have attracted prime attention as promising alternative cathode materials for sodium and lithium

ion batteries, respectively, on the basis of their three-dimensional (3D) framework, good thermal stability, and remarkable electrochemical properties. Recently, a novel lithium transitional bimetal fluoro-phosphate with a highly ordered cations of V<sup>3+</sup> and Fe<sup>3+</sup>, viz. LiV<sub>0.5</sub>Fe<sub>0.5</sub>PO<sub>4</sub>F, was developed by our group and exhibited a single-phase solid-solution behavior over the entire lithium composition range of Li<sub>1-x</sub>V<sub>0.5</sub>Fe<sub>0.5</sub>PO<sub>4</sub>F (0<x<0.5).<sup>21</sup> Inspired by the high Li<sup>+</sup> conductivity of the fluoro-polyanionic compounds, a stoichiometric fluoro-phosphate analogue, i.e. MgFePO<sub>4</sub>F (MFPF), is herein synthesised via a ball-milling assisted solid-state reaction (further details are elaborated in the supplementary information). In pursuit of high performance cathode materials for rechargeable MB as well as establishing the basic correlation between their crystal structure and Mg storage performance, the synthesis, crystal structure of MFPF and its correlation with the electrochemical properties as cathode material for both Mg and Li batteries are discussed herein.

As shown in Figs. 1a and 1b, scanning electron microscopy (SEM) images of the ball-milled MFPF reveal a uniform particle size distribution centered at ~50 nm. Uniformly-dispersed carbon nanotubes (CNTs) are effective for enhancing the conductivity of the composite materials. Moreover, the addition of ~5wt% CNTs can effectively decrease the interparticles fusion degree and serve as reductive agent to avoid the formation of Fe<sup>3+</sup> during the calcination process. X-ray spectroscopic measurements (see Fig. S1) further confirm that iron is in a divalent (Fe<sup>2+</sup>) state in the as-prepared MFPF and that Fe<sup>2+</sup> is in an octahedral coordination.

The synchrotron X-ray diffraction (SXRD) pattern of MFPF synthesised at 650°C, shown in Fig. 2a, indicates a monoclinic structure fully indexed in the *I*2/a space group, which is isostructural with both triplite and wagnerite phases. The refined atomic parameters obtained from Rietveld refinement of the SXRD pattern are shown in Table S1. An entire Mg/Fe antisite

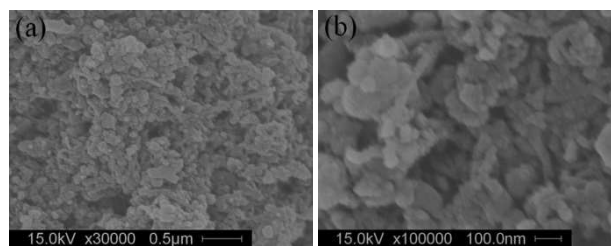


Fig. 1. Scanning electron microscopy (SEM) images at different magnifications for as-prepared MFPF: (a) ×30000 and (b) ×10<sup>5</sup>.

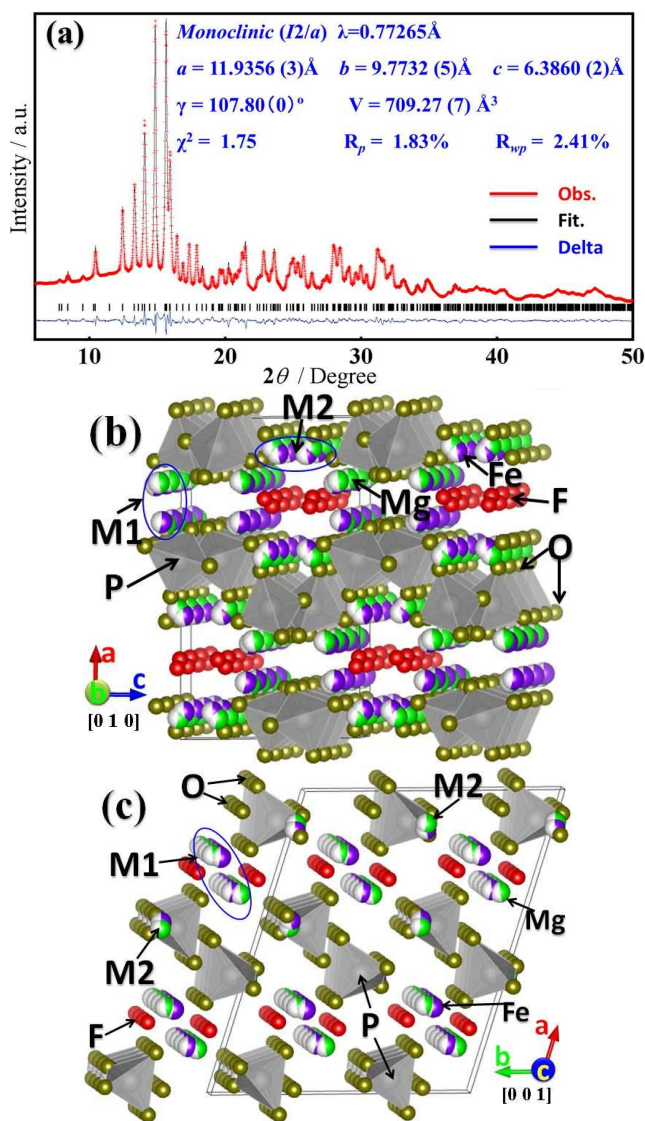


Fig. 2. (a) Rietveld refinement of synchrotron X-ray diffraction pattern of MFPF and the 3D crystallographic representation of monoclinic MFPF projected along (b) [010] and (c) [001].

mixing in the M1 and M2 sites was revealed by the Rietveld refinement results. Its 3D crystallographic representation projected along [010] and [001] is shown in Figs. 2b and 2c, respectively. Furthermore, the monoclinic framework exhibits a unique arrangement of atoms. As shown in Fig. 2 and also Fig. S2, the lattice framework consists of highly distorted octahedrons of  $\text{MO}_4\text{F}_2$  ( $\text{M} = \text{Mg}$  or  $\text{Fe}$ ) and tetrahedrons of  $\text{PO}_4$ . Within the framework, the nearest neighbouring octahedrons at the same M1 or M2 sites share the F–F and O–O edges to form alternating centrosymmetrical octahedron pairs of  $\text{MO}_4\text{F}_2\text{O}_4\text{M}$  and  $\text{F}_2\text{MO}_6\text{MF}_2$ . Consequently, the octahedron chains of cations located at M1 and M2 sites are formed along [010], [001] and so on. Along [010], the F–F edges or bonds serve as bridges to crosslink the octahedron chains of M1 and M2 to form a zigzag octahedron network (see Figs. S2a and S2b). The neighbouring octahedrons at the different sites of M1 and M2 share the F–O edge with each other forming an octahedron pair (i.e.,  $\text{F}_2\text{M1O}_6\text{M2F}_2$ ). The tetrahedral  $\text{PO}_4$  share their vertices with two octahedron pairs ( $\text{F}_2\text{MO}_6\text{MF}_2$ ) and two F–O edge shared octahedron pairs ( $\text{F}_2\text{M1O}_6\text{M2F}_2$ ). Finally, the 3D lattice framework, as seen in Fig. 2b and 2c, is formed.

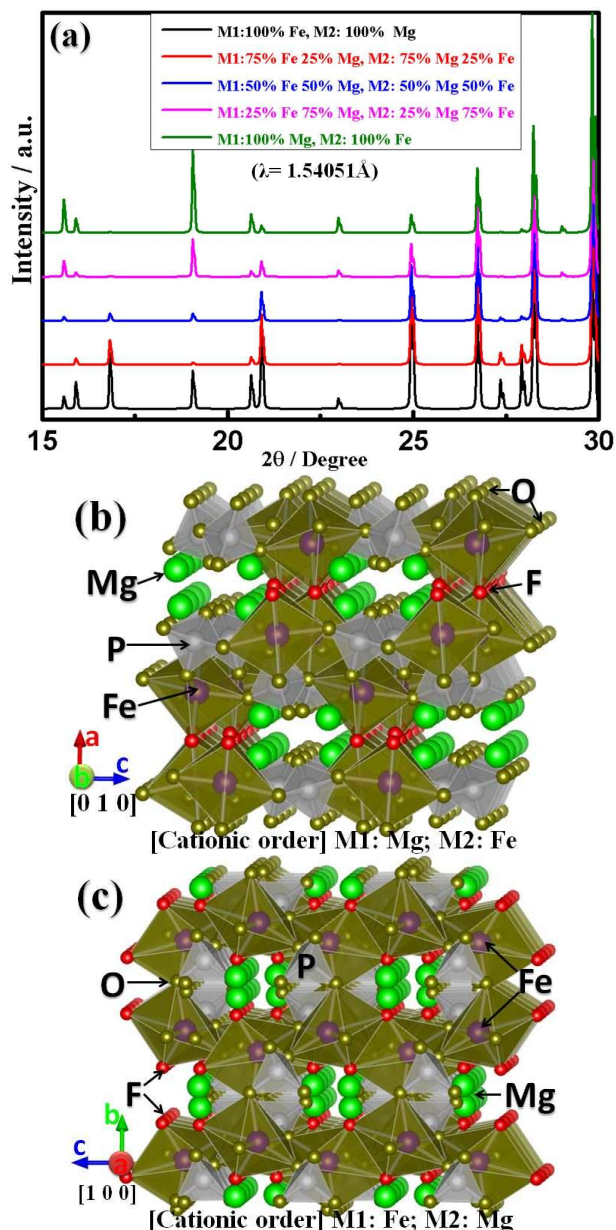


Fig. 3. (a) Simulated X-ray diffraction patterns of MFPF ranging from 15° to 30° with various occupations of Fe and Mg in M1 and M2 sites, while the corresponding 3D crystallographic representations of simulated MFPF in two different cationic orderings are shown in (b) and (c).

To investigate the evolution of crystal structures of MFPF with various occupations of Fe and Mg in M1 and M2 sites, respectively, simulations of their corresponding XRD diffraction patterns were conducted by using the lattice parameters and crystallographic information data obtained from Rietveld refinement of the experimental data. As are apparent in Fig. 3 and Fig. S3, the simulated XRD patterns of MFPF varies with the change of site occupations of M1 and M2. The diffraction pattern of simulated MFPF with Fe and Mg antisite occupations of ca. 50% in both M1 and M2 sites coincides with the observed pattern of as-prepared MFPF (see Fig. S3a and Fig. S4). The simulation results further confirm the immense Mg/Fe antisite mixing

intrinsic in the obtained monoclinic framework derived from the Rietveld refinement analyses. This phenomenon is ascribed to the similarity in ionic radii of  $\text{Mg}^{2+}$  (0.72 Å) and  $\text{Fe}^{2+}$  (0.78 Å), akin to that observed in the fayalite- $\text{MgFeSiO}_4$ .<sup>6</sup> It is important to point out that wide 3D channels for migration of  $\text{Mg}^{2+}$  could obviously be observed from the simulated cationic orderings of MFPP. As shown in Fig. 3b and Fig. S3b, when the M1 and M2 sites are fully occupied by  $\text{Mg}^{2+}$  and  $\text{Fe}^{2+}$ , respectively, wide channels for  $\text{Mg}^{2+}$  to traverse could be found along [010] and [001]. Analogous migration channels for  $\text{Mg}^{2+}$  can also be observed along [100] and [111] whereby  $\text{Fe}^{2+}$  and  $\text{Mg}^{2+}$  occupy M1 and M2 sites, respectively (see Fig. 3c and Fig. S3c).

To further understand the effect of calcination temperature on the crystal structure of MFPP, various calcination temperatures ranging from 600 °C to 850 °C were used to prepare MFPP. As presented in Fig. S4, all corresponding XRD patterns are similar. The crystal grain sizes of MFPP increase from ~24 nm following a near-linear relationship of the grain size increment versus the increase in sintering temperature, see Fig. S6. No obvious correlation could be found between the calcination temperature and the anti-site mixing degree within MFPP. Rietveld refinement of the sample synthesized at 800 °C also indicates an entire Fe / Mg anti-site mixing (see Fig. S5 and Table S2). We are aware that anti-site mixing may impose a limitation in the (de) intercalation of cations; however, the 3D framework conferred by MFPP may be beneficial to allow cations to traverse easily.

As a proof-of-concept, the feasibility of using MFPP as cathode material for MB was examined in a three-electrode cell configuration. The composite electrodes prepared from MFPP were used as the working electrodes. Room-temperature galvanostatic measurements were carried out between -1.2 V and 1.5 V vs.  $\text{Ag}/\text{Ag}^+$  at current densities corresponding to C/20 and C/30 rate. In order to obtain stable electrochemical performances both in Mg- and Li-ion cells, a pre-charge/discharge process was performed to promote ingress of electrolyte into composite electrodes and separators. As is shown in Fig. 4, the subsequent charge / discharge profiles neatly superimpose to attain stable cyclic performance. MFPP exhibits a reversible capacity of 35  $\text{mAhg}^{-1}$  at C/20 rate in a Mg-ion cell (see Fig. 4a and Fig. S8a). A discharge capacity of approximately 53  $\text{mAhg}^{-1}$  could be attained in a Mg-ion cell (see Fig. S7a), which is relatively lower than the sustainable capacity of ca. 86  $\text{mAhg}^{-1}$  achieved in a Li-ion cell (Fig. 4b and Fig. S8b) at the same current density corresponding to C/30 rate. Cyclic performance and coulombic efficiency of the as-prepared MFPP electrodes are given in Fig. S8. The relatively lower coulombic efficiency of MFPP electrode in 0.5M  $\text{Mg}(\text{TFSI})_2$  electrolyte should be ascribed to electrolyte-related side reactions upon charging the electrode to high potential region (see the differential capacity  $dQ/dV$  plots shown in Fig. S9a). Additionally, the electrochemical performance of a control electrode consisting of carbon (acetylene black) and binder (PTFE) is shown in Fig. S7b. The obtained small capacity of 5  $\text{mAhg}^{-1}$  corresponds to the supercapacitive behaviour of carbon.

It is also interestingly to note that the average working potentials are ~2.6 V vs.  $\text{Mg}/\text{Mg}^{2+}$  and ~3.1 V vs.  $\text{Li}/\text{Li}^+$ . To the best of our knowledge, this potential is higher than that reported in most cathode materials for MB.<sup>4-17</sup> The potential exhibited is also slightly higher than that of the  $\text{Fe}^{2+}/\text{Fe}^{3+}$  redox couple in

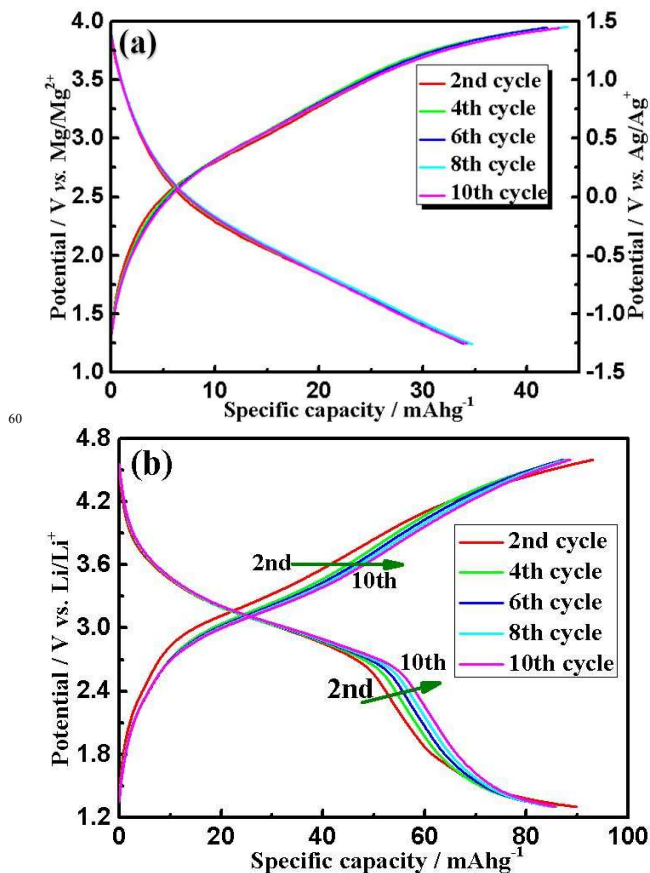


Fig. 4. Voltage (dis)charge profiles of MFPP recorded at 25°C in (a) MB at C/20 rate and (b) LIB at C/30 rate.

$\text{LiFePO}_4\text{F}$  (2.75 V) due to the higher charge/radius ratio of  $\text{Mg}^{2+}$  than that of  $\text{Li}^+$ .<sup>19</sup> The sloping voltage (dis)charge profiles of MFPP in both Mg- and Li-ion cells suggest a solid-solution (single-phase) behaviour, which is distinct from the two-phase behaviour exhibited in  $\text{LiFePO}_4\text{F}$ .<sup>19</sup> As presented in Fig. S9, one pair of oxidation/reduction peaks can be found from the differential capacity  $dQ/dV$  plots corresponding to the tenth charge/discharge cycle of the as-prepared MFPP electrodes in the three-electrode Mg cell (Fig. S9a) and the two-electrode lithium cell (Fig. S9b). The extremely broad oxidation and reduction peaks, instead of extremely narrow and sharp peaks, are characteristic of a single-phase electrochemical behaviour of MFPP in both Mg and Li ion cells.<sup>22, 23</sup> Furthermore, a smaller polarization and more distinct plateaus can be found from the voltage (dis)charge profiles of MFPP in Li-ion than in Mg-ion cell. This could also be confirmed by the smaller peak-to-peak voltage difference between the oxidation and reduction peaks observed from the  $dQ/dV$  plots of lithium ion batteries (~0.17V) than that of Mg batteries (~0.93V). The much wider peak-to-peak separation of  $dQ/dV$  curves of MFPP in Mg system than that of Li system should be ascribed to the stronger interactions with the anions and the cations of the hosts, as well as the much sluggish solid-state diffusion of  $\text{Mg}^{2+}$  cations than that of  $\text{Li}^+$  within the disordered host crystal structure of MFPP arising from higher charge-to-radius ratio of  $\text{Mg}^{2+}$  than that of  $\text{Li}^+$ .<sup>1</sup> Moreover, it is worth noting that the contribution of charge/discharge capacity from the electrochemical double layer capacitance (EDLC) is very limited. As shown in Fig. S7, the capacity of as-prepared composite electrode and acetylene black stemming from EDLC is lower than 10  $\text{mAhg}^{-1}$  and 5  $\text{mAhg}^{-1}$ , respectively. Moreover, the achieved discharge capacity based on MFPP only is ~53  $\text{mAhg}^{-1}$

close to 38.4% of the theoretical capacity of MFPP (138 mAhg<sup>-1</sup>). Thus, merely the surface process, including EDLC and pseudocapitance (resulting from the surface (de)intercalation of Mg<sup>2+</sup>), seems not able to provide such capacity. In view of this, most of the capacity of the composite electrodes stem from the redox reaction of Fe<sup>2+</sup>/Fe<sup>3+</sup> caused by the (de)intercalation of Mg<sup>2+</sup>, as confirmed by the differential capacity dQ/dV plots shown in Fig. S9a. In other words, a limited extraction/intercalation of Mg<sup>2+</sup> from/into the host structure of MFPP take place during the charge/discharge process even though the full intercalation is limited by the entirely cationic mixing of Fe<sup>2+</sup>/Mg<sup>2+</sup> within the crystal structure of MFPP (which block the migration pathways for Mg<sup>2+</sup> diffusion of Mg<sup>2+</sup>) and the sluggish solid state diffusion kinetics of Mg<sup>2+</sup>. Therefore, judicious design of a cationic ordered MFPP possessing straight pathways for the 3D migration of Mg<sup>2+</sup>, as presented in Figs. 3b and 3c, might be essential to further improve the electrochemical performance of MFPP.

In summary, stoichiometric MgFePO<sub>4</sub>F was successfully synthesized using a solid-state carbothermal method. The experimental and simulated XRD results confirmed that the obtained monoclinic MFPP exhibit immense Mg<sup>2+</sup>/Fe<sup>2+</sup> antisite mixing, which in turn results in the relative low utilization ratio and capacity of MFPP. Nonetheless, the relatively high potential (~2.6 V vs. Mg/Mg<sup>2+</sup>) augmented with the good cyclic stability at an encouraging capacity (~60 mAhg<sup>-1</sup>) deem MFPP a promising high voltage cathode material contender for rechargeable magnesium batteries. A reduction of the Mg<sup>2+</sup>/Fe<sup>2+</sup> antisite mixing degree by use of a proper synthetic strategy as well as cycling at elevated temperature could be a necessary prelude to anticipating profound electrochemical performance in MFPP. Such efforts are subject of our future work, as are investigations relating to the mechanism of Mg<sup>2+</sup> (de) intercalation.

## Acknowledgement

This work was supported by CREST project of the Strategic Basic Research Programs of JST.

## Notes and references

<sup>a</sup> Graduate School of Human and Environmental Studies, Kyoto University, Yoshida-nihonmatsu-Cho, Sakyo-ku, Kyoto 606-8501 Japan

Tel: +81 75 7537903; E-mail:hzd0506127@gmail.com

<sup>b</sup> Office of Society-Academia Collaboration for Innovation, Kyoto University, Gokasho, Uji 611-0011, Japan

<sup>c</sup> Graduate School of Engineering, Kyoto University, Katsura-chu, Nishikyo-ku, Kyoto 615-8510

† Electronic Supplementary Information (ESI) available: [details of experimental process and additional results are included here].

- 1 E. Levi, Y. Gofer, D. Aurbach, Chem. Mater., 2010, 22, 860–866.
- 2 H.D. Yoo, I. Shterenberg, Y. Gofer, G. Gershinsky, N. Pour, and D. Aurbach, Energy Environ. Sci., 2013, 6, 2265–2279.
- 3 D. Aurbach, Z. Lu, A. Schechter, Y. Gofer, H. Gizbar, R. Turgeman, Y. Cohen, M. Moshkovich and E. Levi, Nature, 2000, 407, 724.
- 4 A. Mitelman, M. D. Levi, E. Lancry, E. Levi, D. Aurbach, Chem. Commun., 2007, 4212–4214.
- 5 E. Lancry, E. Levi, Y. Gofer, M. D. Levi, D. Aurbach, J. Solid. State. Electrochem., 2005, 9, 259–266.
- 6 Y. Li, Y.N. Nuli, J. YANG, T. Yiliner, J. L. Wang, Chinese Sci. Bull., 2011, 56, 4–5.
- 7 Y.N. Nuli, J. Yang, Y.S. Li and J.L. Wang, Chem. Commun., 2010, 46, 3794–3796.

- 8 Z. Feng, J. Yang, Y.N. Nuli, J.L. Wang, J. Power Sources, 2008, 184, 604–609.
- 9 Y.P. Zheng, Y.N. Nuli, Q. Chen, Y. Wang, J. Yang, J.L. Wang, Electrochimica Acta 2012, 66, 75–81.
- 10 L. F. Jiao, H.T. Yuan, Y.C. Si, Y.J. Wang, Y.M. Wang, Electrochem. Commun., 2006, 8, 1041–1044.
- 11 D. Imamura, M. Miyayama, M. Hibino, and T. Kudo. J. Electrochem. Soc., 2003, 150, A753–A758.
- 12 R.G. Zhang, X.Q. Yu, K.W. Nam, C. Ling, T.S. Arthur, W. Song, A.M. Knapp, S.N. Ehrlich, X.Q. Yang, M. Matsui, Electrochem. Commun., 2012, 23, 110–113.
- 13 S. Rasul, S. Suzuki, S. Yamaguchi, M. Miyayama, Electrochimica Acta, 2012, 82, 243–249.
- 14 Y.L. Liang, R.J. Feng, S.Q. Yang., et al, Adv. Mater., 2011, 23, 640–643.
- 15 Y.C. Liu, L.F. Jiao, Q. Wu, Y.P. Zhao, K.Z. Cao, H.Q. Liu, Y.J. Wang, H.T. Yuan, Nanoscale, 2013, 5, 9562–9567.
- 16 Z.L. Tao, L.N. Xu, X.L. Gou, J. Chen, H.T. Yuan, Chem. Commun., 2004, 2004, 2080–2081.
- 17 B. Liu, T. Luo, G.Y. 8058 Mu, X.F. Wang, D. Chen, G.Z. Shen, ACS Nano., 2013, 7, 8051–8058
- 18 A. Langrock, Y.H. Xu, Y.H. Liu, S. Ehrman, A. Manivannan, C.S. Wang, J. Power Sources, 2013, 223, 62–67.
- 19 B. L. Ellis, L. F. Nazar, Chem. Mater., 2012, 24, 966–968.
- 20 J. M. A. Mba, C. Masquelier, E. Suard, L. Croguennec, Chem. Mater., 2012, 24, 1223–1234.
- 21 Z.D Huang, Y. Orikasa, T. Mase, K. Yamamoto, T. Mori, T. Minato, Y. Uchimoto, RSC Adv., 2013, 3, 22935–22939.
- 22 J. Kim, H. Kim, I. Park, Y.U. Park, J.K. Yoo, K. Y. Park, S. Lee and K. Kang, Energy Environ. Sci., 2013, 6, 830–834.
- 23 G. N. Zhu, L. Chen, Y. G. Wang, C. X. Wang, R. C. Che, Y. Y. Xia, Adv. Funct. Mater., 2013, 23, 640–647.